THREE DIMENSIONAL ANALYSES OF DEEP EXCAVATION IN TAIPEI 101 CONSTRUCTION PROJECT

Der-Guey Lin [1] and Siu-Mun Woo [2]

ABSTRACT

Based on the actual construction sequences, a three-dimensional (3-D) deformation analysis incorporated with steady state groundwater seepage calculation was performed to simulate the ground movement of deep excavation in Taipei 101 (or Taipei International Financial Corporation, TIFC) construction project. In 3-D analysis, an optimized geometry model and mesh density was adopted according to the convergence study to achieve a computation with high efficiency and accuracy. This paper evaluates the lateral wall movement of diaphragm wall considering the restraint effect of wall corner which frequently influenced by the stiffness of strutting system. A value of PSR (Plane Strain Ratio) defined by the ratio of the maximum lateral wall movements from 3-D and 2-D (two-dimensional) analyses in sequential excavation stage is used to quantify the potential of restraint effects. According to the PSR values at Tower zone and Podium zone, the numerical results reveal that the lateral wall movement of all sections being evaluated along diaphragm wall can be restrained by the wall corner during the excavation even though a heavily supporting system was installed. Conclusively, the restraint effect of wall corners is hardly suppressed by the preloaded steel strutting system of bottom-up method at Tower zone and the concrete floor slab strutting system of top-down method at Podium zone and it is exceedingly crucial using 3-D computation model to reflect the realistic deformation behavior of multi-strutted deep excavation in Taipei 101 construction project.

Key words: Three-dimensional analysis, plane strain ratio, restraint effect, stiffness of strutting system.

1. INTRODUCTION

This paper attempts to evaluate the lateral wall movement of deep excavation in Taipei 101 construction project from the view point of interactive mechanism between the restraint effect of wall corner and the stiffness of supporting system. In the previous studies, the restraint effect of wall corner on the lateral wall movement in deep excavation was indicated to be related to the wall length-to-excavation depth ratio of the excavation L/H, the depth to a relatively stiff stratum from excavation bottom, and the overall stiffness of the strutting system K_{ave} which is obtained by dividing the total axial stiffness of all struts bearing on the wall ($\sum E_i \times A_i/L_i$) by the wall area (A) (or $K_{ave} = (\sum E_i \times A_i/L_i)/A$). Nevertheless, it should be noted that the restraint effects of wall corner on lateral wall movement can be suppressed or compensated by a heavily strutting system during excavation.

Based on the numerical analyses conducted by Simpson (1992), a fairly uniform pattern of wall movement was observed at a top-down excavation ($L/H \cong 3.3$) in London Clay using diaphragm wall supported by concrete slabs ($K_{ave} \cong 27$) and restrained effects are insignificant. In the analyses, plane strain and axis-symmetric analyses displayed similar results and these are attributed to the shallow depth of stiff soil stratum. The maximum lateral wall movement occurred below the excavation level because of a relatively thick soft clay layer underlying the excavation level and corner effects there could not be suppressed by the strutting system.

Five case histories of top-down deep excavation ($L/H \cong 2.1$ to 6.0) using diaphragm wall supported by concrete floor slab in typical Taipei subsoil were analyzed by Wong and Patron (1993). It was indicated the ground settlement increased from corner towards the mid-span of excavation and this implies the presence of restraint effect of wall corner. It was also revealed that restraint effects may occur at a wall section situated at a distance of one or less the excavation depth ($\leq 1 \times H$) from corner conjunction. However, it becomes uncertain if the restraint effect were observed on the walls with the larger L/H ratios. Moreover, Ou, *et al*. (1993) performed a series of 2-D and 3-D numerical analyses on a top-down excavation ($L/H \cong 1.0$ to 1.5) using diaphragm wall supported by concrete slabs in Taipei Metropolitan. The soil profile illustrates a medium to stiff silty clay interleaved by layers of silty sand. It was indicated that significant restraint effects occur at the cross section of diaphragm wall located at a distance d of one excavation depth ($d = 1 \times H$) away from wall corner.

Ou, *et al*. (1996) defined a Plane Strain Ratio (PSR = $(\delta_{hmax})_{3D}/(\delta_{hmax})_{2D}$) for a evaluated section of diaphragm wall to quantify the restraint potential of wall corner. In which, $(\delta_{hmax})_{3D}$ and $(\delta_{hmax})_{2D}$ denote the maximum lateral wall movements from 3-D and 2-D analyses at certain excavation stage. The cross section being evaluated with higher PSR value represents the section is less restrained by wall corner and it may approach to plane strain condition as the PSR value becomes unity. The wall being evaluated is called primary wall (with wall width of L_p) whereas the wall conjoined with the primary wall at the corner is called secondary wall (with wall width of L_s). For an intermediate to large width of primary wall (L_p = 60 m, 80 m, and 100 m), the central section ($d = L_p/2$ = 30 m, 40 m, and 50 m) of primary wall

Manuscript received November 29, 2006; revised April 16, 2007; accepted April 18, 2007.

[1] Associate Professor (corresponding author), Department of Soil and Water Conservation, National Chung-Hsing University, Taichung, 402, Taiwan, R.O.C. (e-mail: dglin@dragon.nchu.edu.tw).

[2] President, Trinity Foundation Engineering Consultants Co., Ltd., Taipei, Taiwan, R.O.C. (e-mail: trinity@ms4.hinet.net).

can only reach plane strain condition under the circumstance of relatively small width of secondary wall ($L_s \leq 20$ m). While for a larger width of secondary wall (20 m < L_s < 100 m), the section being evaluated at primary wall is not possible to approach plane strain condition.

To clarify the 3-D deformation behavior of deep excavation in Bangkok subsoil and propose a simplified estimation method for the lateral wall movement of multi-strutted diaphragm wall, Lin, *et al*. (2003) presented a L_p/L_s ~ PSR ~ d evaluation chart (wall dimension ratio ~ plane strain ratio ~ distance from the corner to a section) to estimate the lateral wall movement from 2-D calculation without involving tedious 3-D analysis. The evaluation chart enables a rapid estimation of the maximum deformation of excavation considering the restraint effect of wall corner as a main influence factor. For Bangkok Subsoil, it is suggested to take the restraint effect into account in deformation prediction if the evaluated section possesses a geometry configuration with (L_p/L_s) < 3.5 and d < 25 m (PSR < 0.9). On the contrary, the restraint effect appears to be insignificant as the section located at a distance d > 25 m and L_p/L_s > 3.5 (PSR > 0.9).

Ou and Shiau (1997) indicated that 2-D plane strain finite element analysis of deep excavation can be affected by the restraint of wall corners and 3-D finite element method can reliably predict the ground movement of the excavation using column type of soil improvement or buttress wall. Furthermore, based on the field observations of case histories, the wall movement at the short wall is smaller than that at the long wall. The wall movement increases with an increasing distance from the wall corner. The studies further verify the restraint effects of wall corner on the excavation behavior.

Liu (1995) carried out several numerical analyses on a bottom-up excavation ($L/H \cong$ 2.5 to 4.0) using sheet pile wall internally cross-braced by steel struts ($K_{ave} \cong 40$) in Singapore. Thick layers of soft marine clay are around the excavation and extending to more than 20 m below the excavation level. Back-analysis of field data using 2-D and 3-D finite element analyses showed that wall movement below excavation level is much better predicted by 3-D analyses whereas 2-D analyses consistently over predicted wall movement. There is no significant difference between 2-D and 3-D calculation result and measurement above excavation level. Significant restraint effects from wall corner were suggested only below excavation level because of the relatively thick soft clay layer extended below the excavation and the restrained effects could not be suppressed by the strutting system.

Lee, *et al*. (1998) performed 2-D and 3-D finite element analyses on a bottom-up excavation ($L/H \cong$ 3.0 to 4.5) using diaphragm wall diagonally braced by struts in Singapore. Soft marine clay is above excavation level and medium-stiff to stiff clayey sand is below excavation level. Restraint effects of wall corner were observed from inclinometer and ground settlement data from the short and long side diaphragm wall above and below excavation level.

In summary, several remarks can be made as follows:

(1) The restraint effects of wall corner appear more significant with the low length-to-depth ratio (L/H) of the excavation.

(2) If stiff soil strata underlying the excavation level, the maximum wall movement is likely to be reached above excavation level, and restraint effect of wall corner may be suppressed if sufficiently stiff strutting systems are used.

(3) If thick soft soil strata underlying the excavation, the maximum wall movement is likely to be reached below excavation level, where the stiffness of the strutting system will be much reduced.

2. FIELD DESCRIPTION AND CONSTRUCTION

Taipei 101 Construction Project possesses a deep excavation at Tower zone and Podium zone with area of 152.20 m × 159.14 m, 5-story basement of 21.7 m deep and 101-story steel reinforced concrete tower building of 508 m high. In addition to the pile loading tests, there totally more than 128 boreholes were drilled for sampling and a series of high quality laboratory tests and field tests were conducted to determine the physical and mechanical properties of soil strata. Moreover, a well-organized instrumentation system was also established to monitor various ground responses and structural performances during the excavation. Figure 1 illustrates the plan view of excavation layout of the construction project. As displayed in the layout, the Tower zone was excavated by bottom-up method firstly and the Podium zone excavation was initiated subsequently by top-down method. Taking the mesh generation and computation efficiency into account, merely the area of 43.5 m × 49 m at South-Eastern corner of Tower zone and the area of 30 m × 76 m at North-Western corner of Podium zone were selected for 3-D numerical analyses. Moreover, the sections oriented in N-S and W-E directions were used for two-dimensional (2-D) analyses. Table 1 summarizes the details of the construction project.

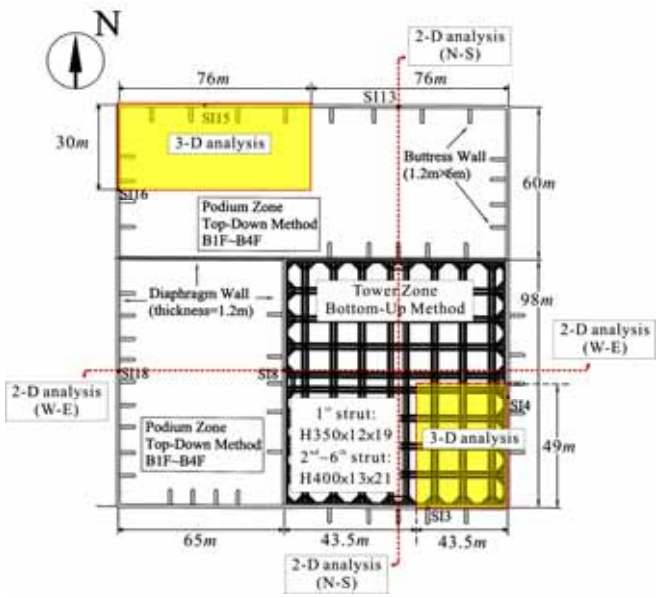

Fig. 1 Excavation configuration and selected zones and sections for numerical analyses

Table 1 Brief of deep excavation of Taipei 101 construction project

Location	Shin Yi District of Taipei Metropolis
Construction period	August 1999 ~ April 2002
Basement geometry	Rectangular
Basement dimension	Tower zone: 98.39 m × 87.10 m Podium zone: 98.39 m × 65.10 m and 152.20 m × 60.75 m
Number of story	Structure: 101-story ; Basement: 5-story
Depth of excavation	Tower zone: 21.7 m ; Podium zone: 21.65 m
Diaphragm wall	Length: 40, 41, 42, 43, 44, 45, and 55 m (depends on the depth of bed rock) Thickness: 1.2 m
Construction method	Tower zone: bottom-up method with preloaded steel strut Podium zone: top-down method with concrete floor slab

3. INSTRUMENTATION

The instrumentation mainly consisted of inclinometers, settlement points, piezometer and rebar strain gauges. The detail layout of instrumentation is shown in Fig. 2 and the selected instrumentations for numerical comparison are tabulated in Table 2.

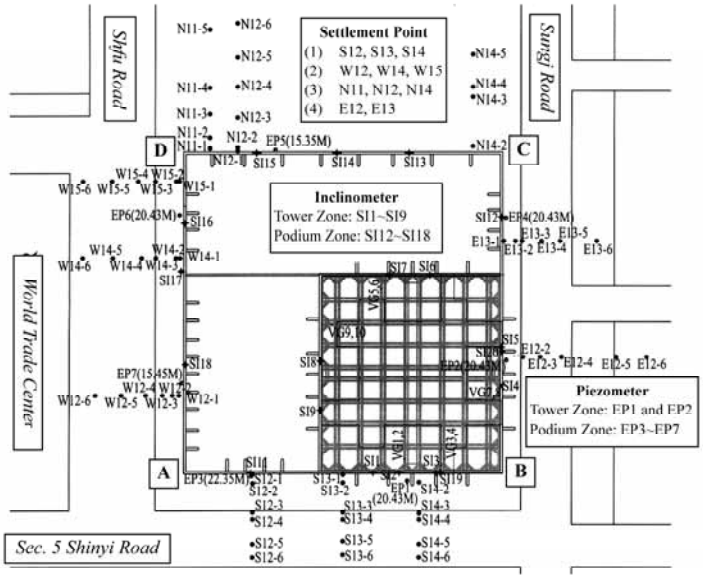

Fig. 2 Configuration of instrumentation points specified by corners A, B, C, and D

Table 2 Instrumentation selected for numerical calibration

Inclinometer		**Location**		
SI3		32 m from Corner-B at Tower zone		
SI16		30 m from Corner-D at Podium zone		
Settlement point		**Location**		
S14		32 m from Corner-B and 4.5 m from Diaphragm wall		
W15		15 m from Corner-D and 2 m from Diaphragm wall		
Piezometer		**Location**	**Installation depth (m)**	
EP1-1	EP1-2	47 m from the Corner-A	20.0	39.1

4. SUBSOIL INVESTIGATION

Lin (2000) and Woo (2005) have investigated the soil strata of jobsite and summarized the required soil properties for numerical analyses according to 128 boring logs (AH-1 ~ AH-15, B-1 ~ B-5, C-1 ~ C-12, D-1 ~ D-89, E-1 ~ E-17) with high quality field test and laboratory test. For field tests, SPT-N value test, vane shear test, geophysical exploration and in-situ permeability test were conducted to obtain the strength parameters and permeability of soil layers. For laboratory tests, classification test, consolidation test, triaxial UU, CIU, CK_oU-AC tests, uniaxial compression test and permeability test were encompassed. The typical subsoil profile of the construction project is mainly composed of alternating silty clay (CL) and silty sand (SM) deposits. In general, the alluvium layer or sandstone layer (SS) can be encountered at an average depth of 45.5 m. Moreover, the ground water table fluctuated around an average elevation of 2 m below the ground surface and which was adopted for the initial condition of seepage analysis.

5. NUMERICAL MODELING

5.1 Finite Difference Discretization

In 3-D numerical analysis, a soil mass can be discretized into two different configurations (overlay 1 and 2) of eight-node zone block and each block consists of five tetrahedral elements internally as shown in Fig. 3. The calculation of nodal forces can be carried out using a combination of two overlays and evaluated by averaging over the two overlays.

Beam elements were used to model the steel strut of bottom-up construction at Tower zone in which bending resistance and limited bending moments occur when loaded by earth pressure or preloading. The element is a two-node, straight finite element with six degrees of freedom per node: three translational components and three rotational components as shown in Fig. 4(a). In addition, shell elements were used to model the diaphragm wall and the floor slabs of top-down construction at Podium zone in which the forces and bending moment caused by earth pressure can be calculated. The element is a three-node, flat finite elements with six degrees of freedom per node as shown in Fig. 4(b).

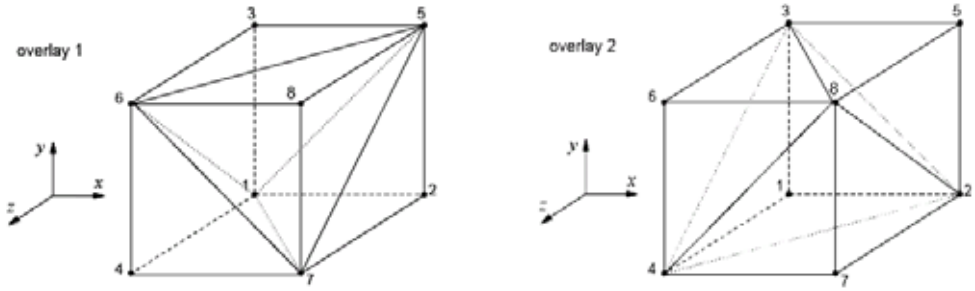

Fig. 3 An eight-node zone block with two overlays of five tetrahedral in each overlay

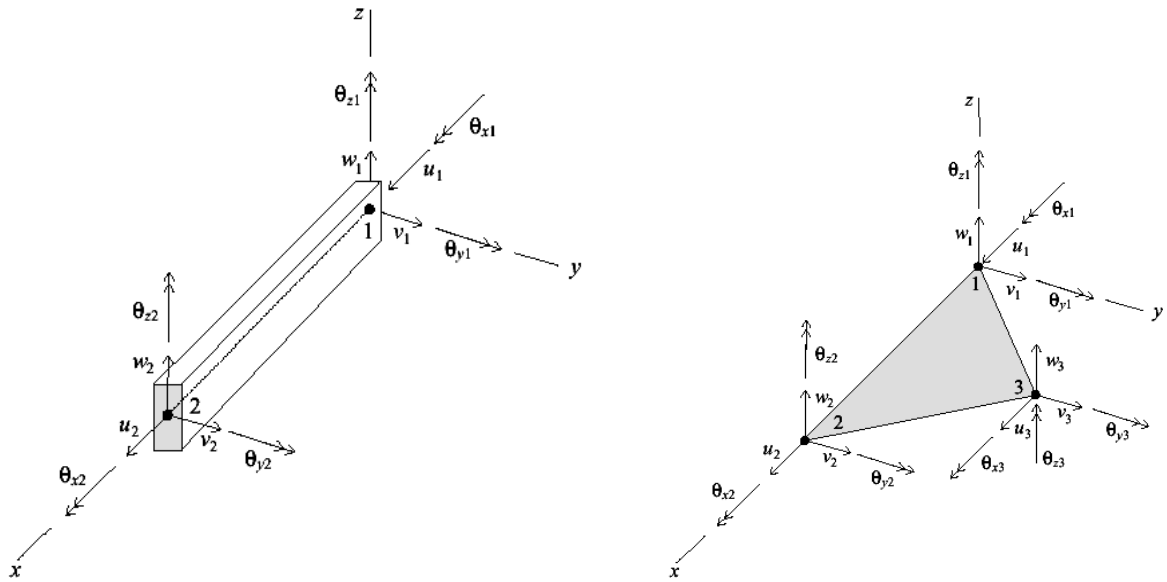

(a) beam element (b) shell element

Fig. 4 Local coordinate and degree of freedom

5.2 Geometry Model

Peck (1969) compiled the result of observation in excavation found that the convergence boundary can be located at a distance of 3 times excavation depth ($3 \times H$) from the retaining structure. Lin, *et al*. (2003) performed a series of convergence study on a hypothetical excavation in Bangkok Subsoil to verify the effect of geometry boundary on numerical accuracy and computational efficiency. For a 30 m × 30 m of excavation dimension and 10 m of excavation depth, the geometry boundary located at a distance of three times excavation depth ($3 \times H$) from the diaphragm wall can lead to a fast convergence of lateral wall movement and ground settlement without sacrificing the accuracy. The bottom boundary of the geometry model was placed on the sandstone layer which situated at a depth of 60 to 62 m. Consequently, the optimized geometry model for 3-D numerical analysis of deep excavation in Taipei 101 construction project was determined on the basis of $3 \times H$ with appropriate mesh density for different zones in the model. Table 3 presents the detail of element size for different zones.

As shown in Fig. 1, the area of South-Eastern corner at Tower zone and North-Western corner at Podium zone were selected for 3-D mesh generation. Accordingly, the dimension of entire geometry model is taken to be 109.5 m × 115 m × 62 m ($X \times Y \times Z$) for Tower zone and 142 m × 96 m × 60 m ($X \times Y \times Z$) for Podium zone and the corresponding 3-D finite difference mesh are illustrated in Fig. 5(a) and 5(b). The dimension of excavation zone for final excavation stage is 43.5 m × 49.0 m × 22.0 m ($X \times Y \times Z$) at Tower zone and 76.0 m × 30.0 m × 22.0 m ($X \times Y \times Z$) at Podium zone. Moreover, different prescribed displacement boundary conditions were specified in the geometry model. The bottom boundary was restrained from vertical and horizontal movements, while the side boundaries are free to move vertically but restrained horizontally.

Table 3 Element size for various zones in 3-D finite difference mesh

Zonation	Tower zone		Podium zone	
	Element size (m) ($\Delta X \times \Delta Y \times \Delta Z$)	Dimension (m)	Element size (m) ($\Delta X \times \Delta Y \times \Delta Z$)	Dimension (m)
Zone I (Zone V)	3.6×3×1 (3.6×3×2.5)	$X_1 = 43.5$ $X_2 = 66.0$	3.9×3.75×1.2 (3.9×3.75×2.45)	$X_1 = 76.0$ $X_2 = 66.0$
Zone II (Zone VI)	6×3×1 (6×3×2.5)	$Y_1 = 49.0$ $Y_2 = 66.0$	6×3.75×1.2 (6×3.75×2.45)	$Y_1 = 30.0$ $Y_2 = 66.0$
Zone III (Zone VII)	3.6×6×1 (3.6×6×2.5)	$Z_1 = 22.0$ $Z_2 = 40.0$	3.9×6×1.2 (3.9×6×2.45)	$Z_1 = 22.0$ $Z_2 = 38.0$
Zone IV (Zone VIII)	6×6×1 (6×6×2.5)		6×6×1.2 (6×6×2.45)	

Zones V, VI, VII, and VIII are below the excavation bottom

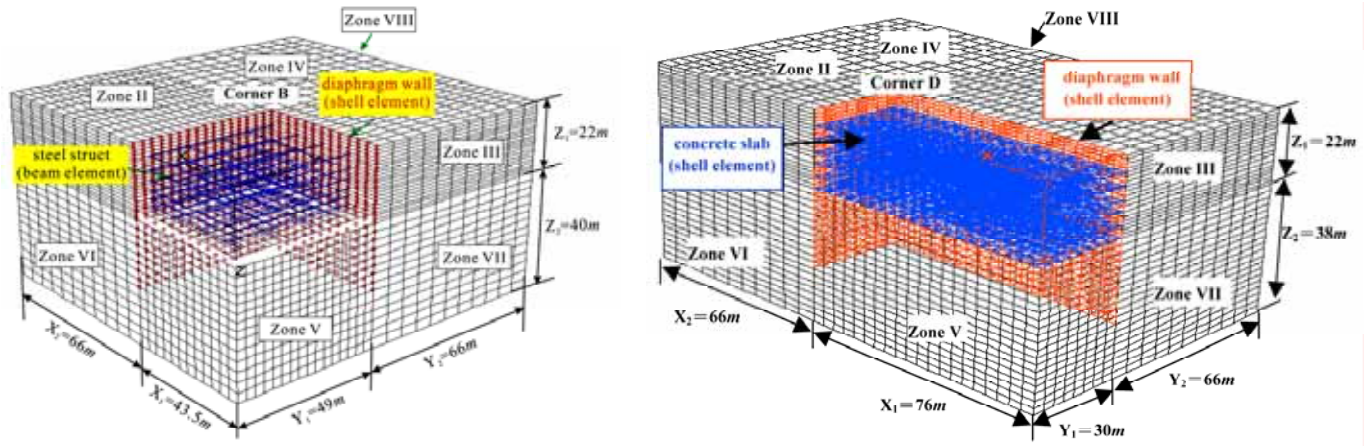

(a) Tower zone (b) Podium zone

Fig. 5 Finite difference mesh of final excavation stage

5.3 Constitutive Model and Model Parameters

In numerical analyses, except the sandstone bearing layer modeled by elastic model the soil mass was assumed to behave as elastic-plastic material and described by Mohr-Coulomb model. The effective stress model parameters c (cohesion), ϕ (friction angle), ν (Poisson's ratio), ψ (dilation angle) and E (elastic modulus) of soil layers were directly obtained from the CIU triaxial compression tests of undisturbed samples (Lin and Woo, 2000). From the test, the E values for soil strata are equivalent to the initial tangent modulus of stress/strain curve which matches with the appropriate confined pressure of depth where soil layer located and the ν values were assumed to range between 0.25 and 0.33. In general, the value of $\nu \leq 0.35$ is adopted to ensure the bulk modulus of pore water K_w must be higher than that of the soil skeleton. The shear modulus G and bulk modulus K of soil layers were calculated by $G = E/2(1 + \nu)$ and $K = E/3(1 - 2\nu)$. Table 4 summarized the effective stress model parameters for numerical calculations.

In the analysis, the concrete and steel structures were both assumed to behave as linear elastic materials with no failure limit. The Young's modulus of the diaphragm wall and the concrete floor slabs were determined by the general formula of concrete material $E_c = 1.46 \times 10^6 (f_c')^{0.5}$ kPa. However, the Young's modulus of the concrete buttress walls was reduced into $0.25 \times E_c$ to cover the possibility of lower construction quality. On the other hand, the Young's modulus of steel strut $E_s = 2.06 \times 10^8$ kPa was determined according to the commonly used steel structure. The required model parameters of structural materials are tabulated in Table 5. The beam element and shell element are assumed to behave as a linear-elastic material with no failure limit and the constitutive relation is isotropic, requiring elastic Young's modulus E_s (or E_c) and Poisson's ratio, ν_s (or ν_c).

Table 4 Effective stress parameters of Mohr-Coulomb model and elastic model

Soil layer	Depth (m)		γ_{wet} (γ_d) (kN/m^3)	K (MPa)	G (MPa)	c (kPa)	ϕ (°)	ψ (°)	σ^t (kPa)
	Tower zone (T)	Podium zone (P)		(T) (P)	(T) (P)	(T) (P)	(T) (P)	(T) (P)	(T) (P)
SF	0 ~ 2.2	0 ~ 1.8	17.16 (13.00)	3.33 4.26	1.53 2.0	2.0 2.0	30 30	0 0	3.46 3.46
CL	2.2 ~ 13.4	1.80 ~ 33.9	17.65 (13.07)	11.1 6.66	4.25 2.5	5.0 5.0	26 26	0 0	10.25 10.25
CL	13.4 ~ 24.5	33.9 ~ 36.0	17.65 (13.07)	39.18 9.22	15 3.47	5.0 10.0	26 30	0 0	10.25 17.32
CL	24.5 ~ 37.0		17.65 (13.07)	99.77 9.22	38.17 3.47	10.0 10.0	30 30	0 0	17.32 17.32
SM	37.0 ~ 42.0	36.0 ~ 40.3	19.12 (15.54)	41.7 4.20	19.2 2.0	5.0 5.0	34 34	1 1	7.41 7.41
CL	42.0 ~ 45.0	40.3 ~ 45.8	18.63 (14.55)	45.2 9.22	17.4 3.47	10.0 10.0	30 30	0 0	17.32 17.32
GC ~ GM	45.0 ~ 48.0	45.8 ~ 49.3	19.41 (15.91)	266 53.2	123 24.5	2.0 2.0	35 35	2 2	2.86 2.86
SS	48.0 ~ 62.0	49.3 ~ 60.0	21.50 (18.8)	370 74.1	222 4.44	–	–	–	–

SF = surface fill, SS = sandstone layer, T = Tower zone, P = Podium zone, σ^t = tensile strength

Table 5 Model parameters of diaphragm wall, concrete floor slab, concrete buttress wall, and steel strut

Element type	Shell element		Beam element	Soil element
Structural dimension	Thickness of diaphragm wall (m)	Thickness of concrete slab (m)	Steel strut (mm)	Concrete buttress wall width × length (m × m)
Specification	1.2	0.15 (floor slab) 3 (mat slab)	H350 ×12 ×19 (1st strut) H400 ×13 ×21 (2nd ~ 6th strut)	7.80 × 3.75 or 7.50 × 3.90
Material strength (kg/cm^2) (MPa)	$f_c' = 210$ (20.60)		$f_y = 2500$ (245.18)	$f_c' = 140$ (13.73)
Unit weight γ (kN/m^3)	23.5		77.1	23.5
Young's modulus E (MPa)	2.13×10^4		2.06×10^5	5.33×10^3
Bulk modulus K (MPa)	1.01×10^4		1.72×10^5	2.53×10^3
Shear modulus G (MPa)	9.30×10^3		7.90×10^4	2.33×10^3
Poisson's ratio v	0.15		0.30	0.15

To calculate the variation of pore water pressure during excavation, a steady state groundwater seepage calculation was performed simultaneously in numerical procedures. The required input parameters are listed in Table 6. In which, the permeability, k, was determined according to the data from laboratory permeability tests and field pumping tests. For the current study, the permeability in horizontal direction k_x and k_y and vertical direction k_z were assumed to be equivalent.

Table 6 Permeability of soil strata for groundwater seepage analysis at Tower zone

Soil layer	Depth (m)		Permeability k ($\times 10^{-8}$ cm /sec)
	Tower zone	Podium zone	
CL	2.2 ~ 24.5	1.8 ~ 33.9	18.06
CL	24.5 ~ 37.0	33.9 ~ 36.0	5.76
SM	37.0 ~ 42.0	36.0 ~ 40.3	2550.0
CL	42.0 ~ 45.0	40.3 ~ 45.8	1.02
GC ~ GM	45.0 ~ 48.0	45.8 ~ 49.3	5170.0
SS	48.0 ~ 62.0	49.3 ~ 60.0	4570.0

5.4 Implementation of 3-D and 2-D Analyses

Prior to the simulation of excavation, the diaphragm wall was assumed to be "wished-in-place" at Tower zone and Podium zone.

The numerical simulation was performed according to the construction sequence of bottom-up method at Tower zone as shown in Fig. 6:

(1) Excavate to −4.4 m (below ground surface) and install the 1st struts at −3.4 m.
(2) Excavate to −8.4 m and install 2nd struts at −7.0 m.
(3) Excavate to −11.3 m and install 3rd struts at −10.3 m.
(4) Excavate to −14.3 m and install 4th struts at −13.3 m.
(5) Excavate to −16.7 m and install 5th struts at −15.5 m.
(6) Excavate to −18.9 m and install 6th struts at −17.7 m.
(7) Excavate to −21.7 m and construct a 3 m thick of concrete mat (from −18.7 m to −21.7 m)

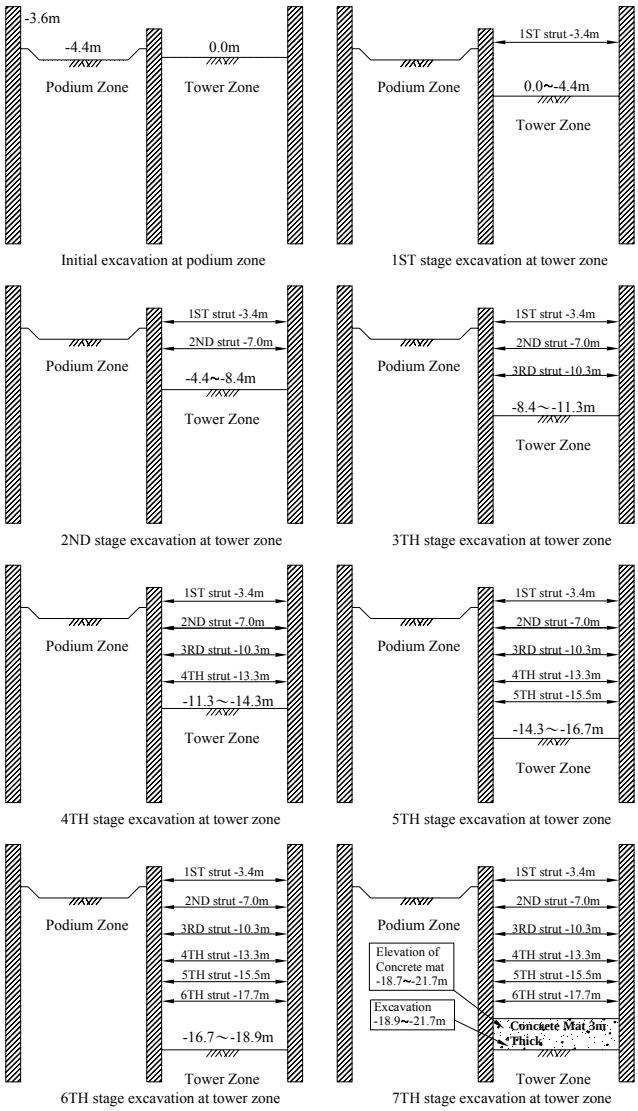

Fig. 6 Construction sequences of excavation at Tower zone (bottom-up method)

In fact, the excavation at Podium zone was initiated after completing the excavation at Tower zone. The numerical simulation was performed according to the construction sequence of top-down method at Podium zone as shown in Fig. 7:

(1) Excavate to −4.4 m (below ground surface).
(2) Excavate to −5.6 m.
(3) Construct B1F (Basement 1st Floor) at –4.4 m and excavate to –10.05 m.
(4) Construct B2F at –8.9 m and excavate to –13.15 m.
(5) Construct B3F at –12.0 m and excavate to –16.25 m.
(6) Construct B4F at –15.1 m and excavate to –18.70 m.
(7) Excavate to –21.65 m.
(8) Construct B5F at –18.04 m and 3 m thick of concrete mat (from −18.65 m to −21.65 m).

However, it should be pointed out the simulation at Podium zone was considered as an independent construction event without any interference with the construction at Tower zone.

In addition to 3-D analysis, a 2-D plain strain analysis was also carried out using the identical numerical tool, input parameters and simulation procedures with those of the 3-D analysis. As shown in Fig. 8, the geometry model for 2-D analysis can be generated simply by assigning a fixity boundary along *Z*-direction (zero displacement in *X*-direction) and using a unit width ($Y_1 = Y_2 = 1$ m) in the *Y*-direction of the 3-D analysis.

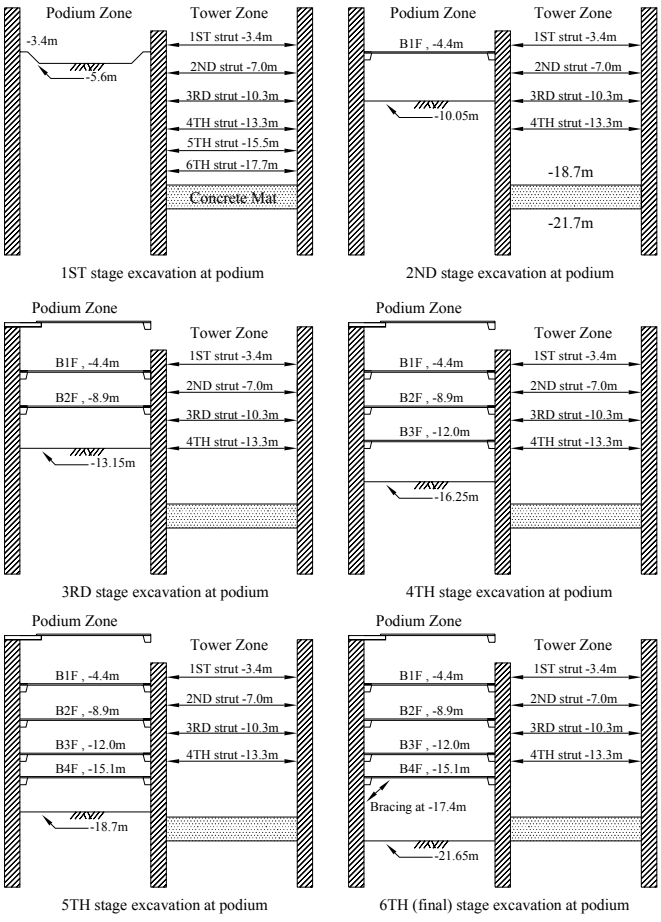

Fig. 7 Construction sequences of excavation at Podium zone (top-down method) after completing the excavation of Tower zone

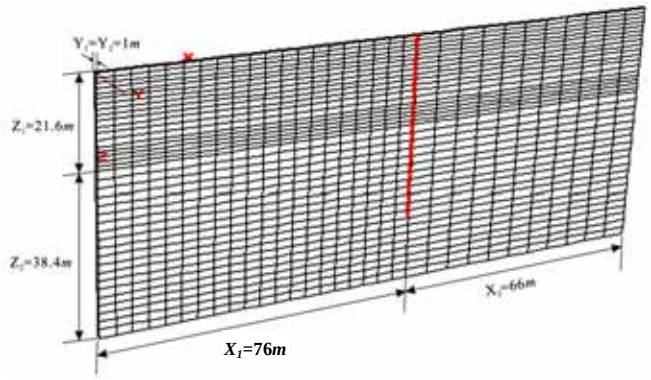

Fig. 8 Finite difference mesh for 2-D plane strain analysis at Podium zone

6. RESULTS AND DISCUSSIONS

6.1 Pore Water Pressure

A groundwater seepage analysis was performed under steady state condition for individual excavation stage at Tower zone and the calculated pore water pressure for a specific excavation stage was plotted with field observation which was varied with elapsed time as shown in Figs. 9(a) and 9(b). The analysis is based on the assumption that the steady seepage flow is sustained within a short period of stage construction for each excavation level. As illustrated in Fig. 2, the observations of EP1-1 and EP2-1 (at depth of −20 m) were adjacent to the excavation bottom (final excavation depth of −21.7 m) and fall in the active zone of earth pressure. On the other hand, EP1-2 and EP2-2 (at depth of −39.1 m) were located at passive zone of earth pressure. For both cases, the predicted pore water pressure shows a descending tendency as the excavation proceeds and which is largely coincident with the observation. In general, the pore water pressure decreases mildly with elapsed time and approach to a steady value. This can be caused either by a seepage drawdown of water table or a lateral unloading of excavation. However, an increasing pore water pressure was found at EP1-1 (at depth of −20 m) during the installation of 2nd (excavation depth of −8.4 m and preloading at −7.0 m), 3rd (excavation depth of −11.3 m and preloading at −10.3 m) and 4th (excavation depth of −14.3 m and preloading at −13.3 m) steel struts. Since the preloading of steel struts was still distant from the EP1-1, thus the increasing pore water pressure can be resulted from the compression of soil mass near excavation bottom due to a cantilever type of lateral wall movement continuously mobilized.

6.2 Ground Movement

As shown in Fig. 10, the observations of ground movement in deep excavation of Taipei 101 construction project were plotted together with the empirical relationship between maximum ground settlement (S_{vm}) and maximum lateral wall movement (D_{hm}) produced by Mana and Clough (1981) and Ou, *et al*. (1998) from data in varied overall ground conditions in San Francisco and Taipei Basin. It was indicated that the empirical relationship of deep excavation in Taipei 101 project appear most likely to be $[S_{vm}/H_e](\%) = (0.5 \sim 1.0) \times [D_{hm}/H_e](\%)$ where, H_e is the excavation depth and the solid curve line from regression calculation can be given by:

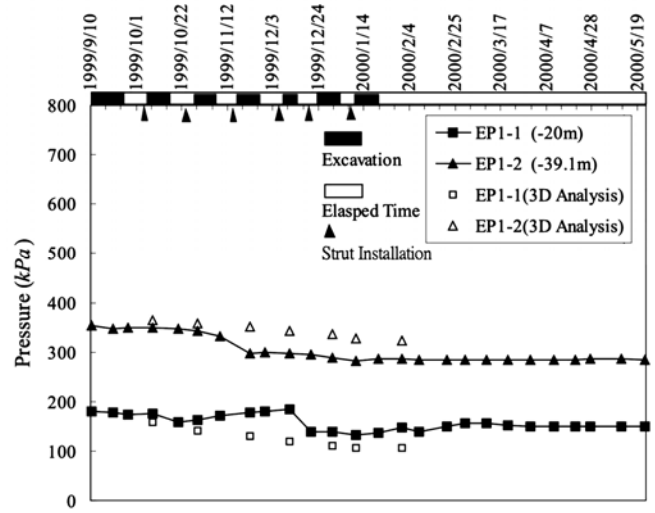

(a) EP1

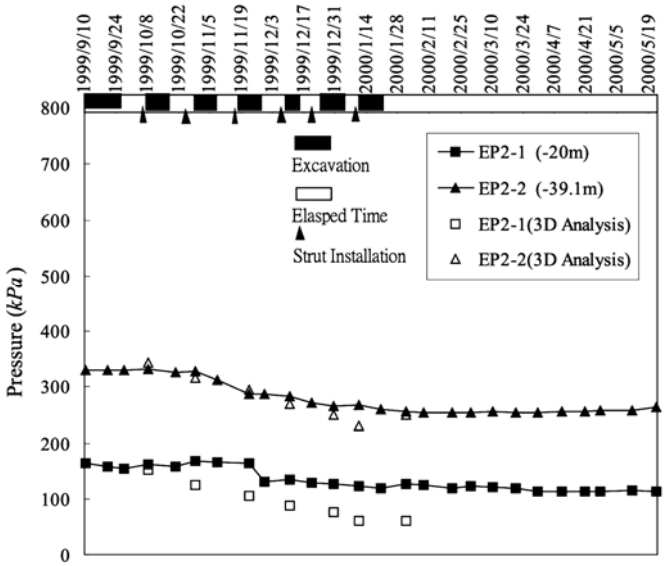

(b) EP2

Fig. 9 Comparisons of pore water pressure between 3-D groundwater seepage analysis and observation at Tower zone

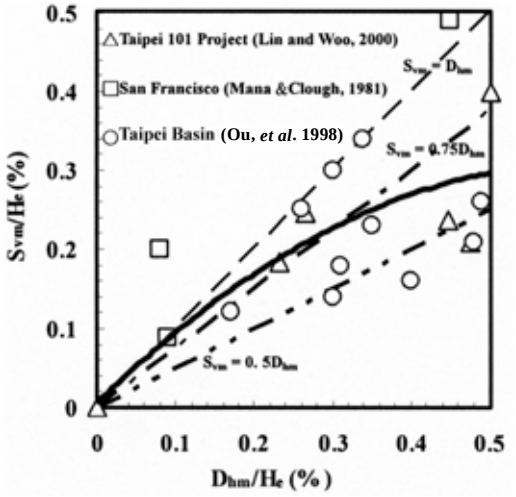

Fig. 10 Empirical relationship between maximum ground settlement and maximum lateral movement

$$[S_{vm}/H_e](\%) = -0.7682\times\{[D_{hm}/H_e](\%)\}^2 + 0.9656\times[D_{hm}/H_e](\%) + 0.0066$$

6.3 Ground Settlement

The ground settlement at final excavation stage was illustrated in Fig. 11, in which, S14 was installed at 4.5 m behind diaphragm wall and aligned across Shinyi Rord. On the other hand, W15 was aligned across Shihfu Road and 2 m distant from diaphragm wall. As can be seen, the numerical prediction underestimates the ground settlement and the deviation can be resulted from the inherent limitation of material models.

6.4 Restraint Effect on Lateral Wall Movement of Deep Excavation

Figures 12 and 13 elaborate the comparisons of lateral wall movement between measurements and calculations at Tower zone and Podium zone for the sequential excavation stage. It is apparent that 3-D analysis is more competent to capture the deformation response of diaphragm wall than 2-D analysis which frequently tends to over predict the lateral movement of the wall section. Simultaneously, the corresponding (L/H) ratio, overall stiffness of strutting system ($\sum E_iA_i/L_i)/A$, maximum lateral wall movement δ_{hmax} and PSR value for various excavation stages are tabulated in Tables 7 and 8.

(1) Tower zone (bottom-up construction with preloaded steel strut)

As shown in Figs. 12(a) ~ 12(g), a bottom-up excavation with dimension of 87 m × 98 m = $L_p \times L_s$) and with preloaded steel strut at Tower zone exhibits a cantilever type of displacement mode and the maximum lateral wall movement always occurs above the excavation level. Unlike the 3-D analysis, the 2-D analysis constantly over predicted the lateral wall movement as the excavation proceeded. However, at final stage the deviation between 3-D and 2-D predictions is comparatively small below the excavation level and this can be resulted from the stiffer silty clay layer (CL) and silty sand layer (SM) underlying the excavation level.

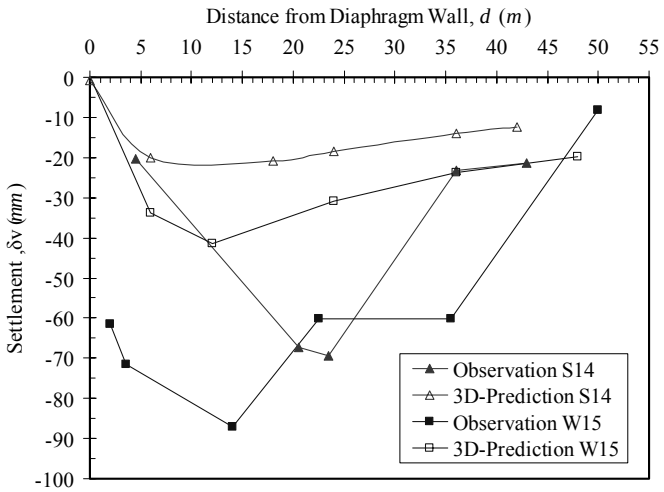

Fig. 11 Comparisons of ground settlement between prediction and observation at final excavation stage (S14 at Tower zone and W15 at Podium zone)

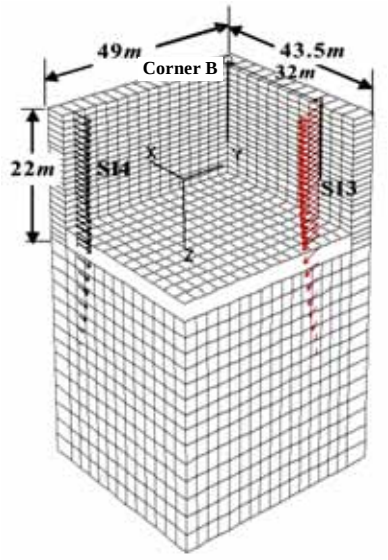

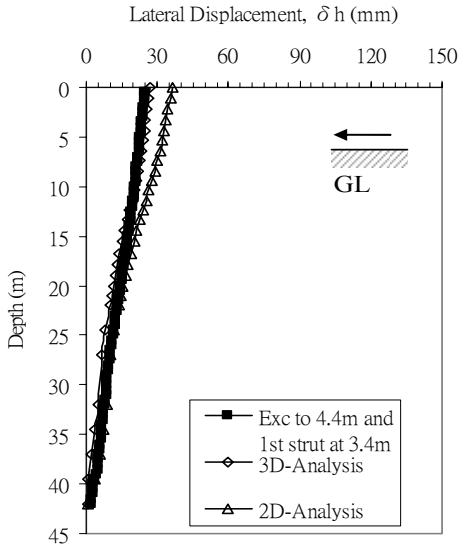

(a) 4.4m

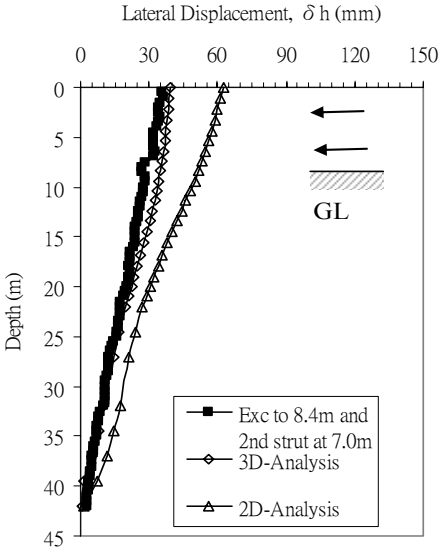

(b) 8.4m

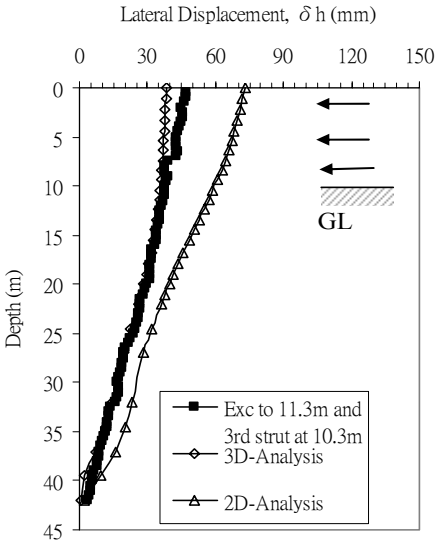

(c) 11.3m

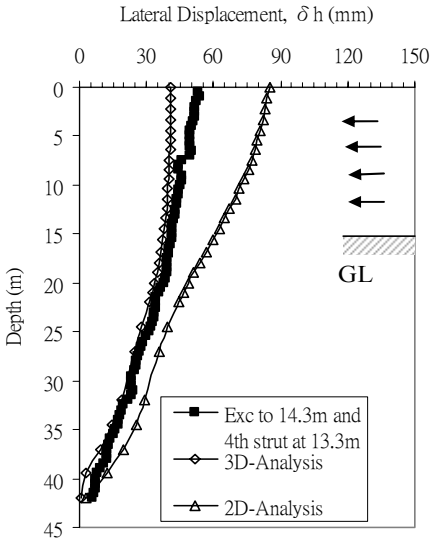

(d) 14.3m

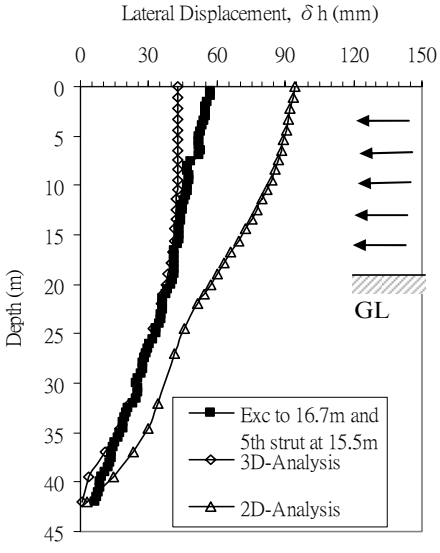

(e) 16.7m

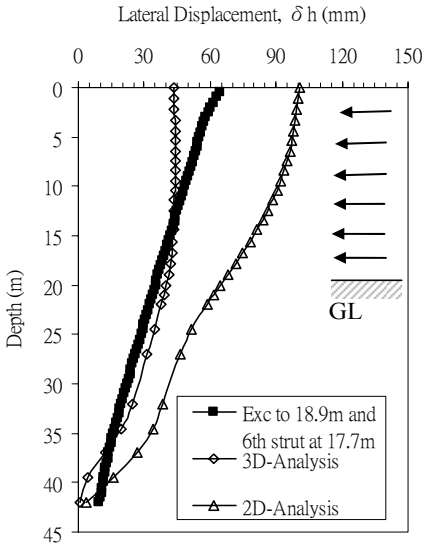

(f) 18.9m

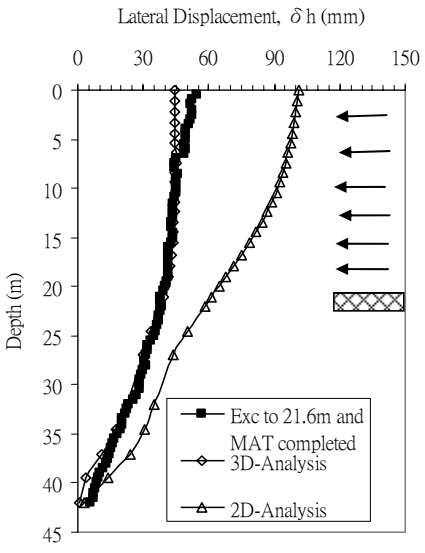

(g) 21.6m

Fig. 12 Comparisons of lateral wall movement of SI3 between measurement and numerical results at Tower zone for various excavation depths *H*

Table 7 Restraint effects on the lateral wall movement of excavation at Tower zone (SI3)

Depth/length ratio of various excavation stage	Strut stiffness $(\sum E_s A_s/L_s)/A$ (kN/m/m^2)	Lateral displacment of diaphragm wall			
		$(\delta_{hmax})_{measured}$ (mm)	$(\delta_{hmax})_{3D}$ (mm)	$(\delta_{hmax})_{2D}$ (mm)	PSR $(\delta_{hmax})_{3D}/(\delta_{hmax})_{2D}$
1st stage (0 ~ −4.4 m) L/H = 10.20	4637 (1st level)	24.93	26.59	36.23	0.73
2nd stage (−4.4 ~ −8.4 m) L/H = 5.35	5483 (1st ~ 2nd level)	35.69	39.34	62.43	0.63
3rd stage (−8.4 ~ −11.3 m) L/H = 3.98	6347 (1st ~ 3rd level)	46.79	38.34	73.21	0.52
4th stage (−11.3 ~ −14.3 m) L/H = 3.14	6810 (1st ~ 4th level)	52.81	40.96	85.16	0.48
5th stage (−14.3 ~ −16.7 m) L/H = 2.70	7368 (1st ~ 5th level)	56.92	42.68	94.08	0.45
6th stage (−16.7 ~ −18.9 m) L/H = 2.38	7868 (1st ~ 6th level)	64.24	43.46	100.84	0.43
7th stage (−18.9 ~ −21.7 m) L/H = 2.07	6.73×10^4 (1st ~ 6th level and 3 m thick concrete mat)	54.25	44.26	101.33	0.44

Steel strutting system at Tower zone:
1st level steel strut: 4 × H350 × 12 × 19 (one strut)
2nd ~ 6th level stell strut: 4 × H400 × 13 × 21(one strut)

(1) Concrete mat with thickness of 3 m was constructed at the final excavation level.
(2) Section properties of steel strut member:
H350 × 12 × 19 (I_x = 40295 cm^4, A_s = 173.87 cm^2)
H400 × 13 × 21 (I_x = 66621 cm^4, A_s = 218.69 cm^2)
(3) Stiffness of supporting system:
$(\sum E_s A_s/L_s)/A$ = overall axial stiffness
E_s = Elastic modulus of steel strut = 2.06×10^8 kPa
A_s = Cross sectional area of strut member
L_s = Length of strut member
I_x = Moment inertia of strut member
A = Wall area supported by steel strut
L = Vertical length of diaphragm wall = 45 m
H = Excavation depth

As listed in Table 7, the PSR value is continuously descending from 0.73 to 0.44 as the L/H ratio decreases from 10.20 to 2.07 and this is caused by the fact that the increasing rate of $(\delta_{hmax})_{3D}$ value is numerically lower than $(\delta_{hmax})_{2D}$ value as the excavation proceeds. Although the overall stiffness of strutting system K_{ave} was maintained at a relatively high level from 4637 to 6.73×10^4 kN/m/m^2 (included 3 m thick of concrete mat) through the entire excavation period, the restraint effect of wall corner on the section SI3 located at a distance d = 32 m (≅ 1.48H > 1.0H) from corner conjunction is still existing and hardly to be suppressed or compensated by strutting system.

(2) Podium zone (top-down construction with concrete floor slab support)

On the other hand, as shown in Fig. 13(a) ~ 13(g), the excavation with dimension of $L_p \times L_s$ = 60 m × 152 m at Podium zone was carried out by top-down construction with concrete floor slab supporting system. The diaphragm wall initially displays a cantilever type of deformation mode and eventually turns into a deep inward bulged type of lateral wall movement. Similarly, 3-D analysis is more competent than 2-D analysis in numerical prediction. Except at cantilever mode, the maximum lateral wall movement at inward bulged mode mostly occurs nearby the excavation level.

Contrary to the Tower zone, as presented in Table 8, the PSR value is increasing from 0.32 to 0.61 in response to the decrease of L/H ratio from 8.06 to 2.08 for the sequential excavation. Numerically this is resulted from the $(\delta_{hmax})_{2D}$ value of large percentage mobilized at the earlier excavation stage due to large unsupported excavation depth −5.7 m at Podium zone in contrast to −4.4 m at Tower zone. Conversely, the $(\delta_{hmax})_{3D}$ value is increasing in a stepwise manner and the increase of PSR value implies the restraint effect of wall corner could be gradually relieved as the excavation proceeds.

Yet a high level of overall stiffness of strutting system K_{ave} ranges from 400 to 3.99×10^6 kN/m/m^2 (included 3 m thick of concrete mat) remains. The restraint effect on the section SI16 located at a distance d = 30 m (≅ 1.39H > 1.0H) from wall corner is still effective.

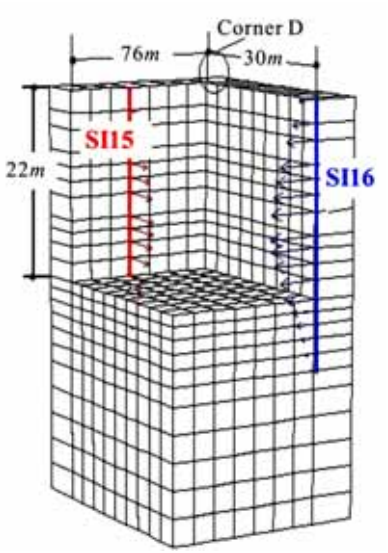

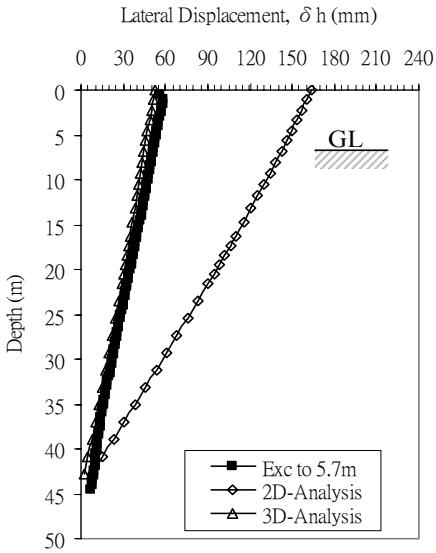

(a) 5.7m

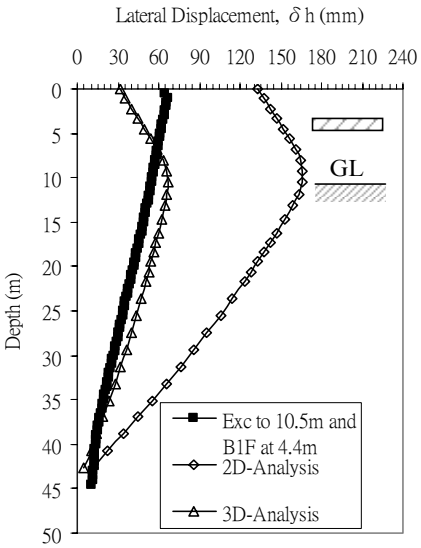

(b) 10.5m

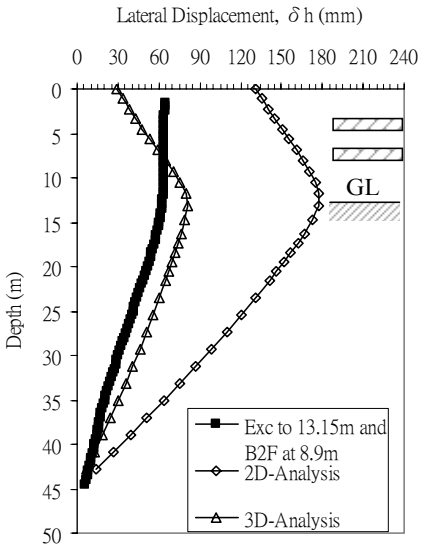

(c) 13.15m

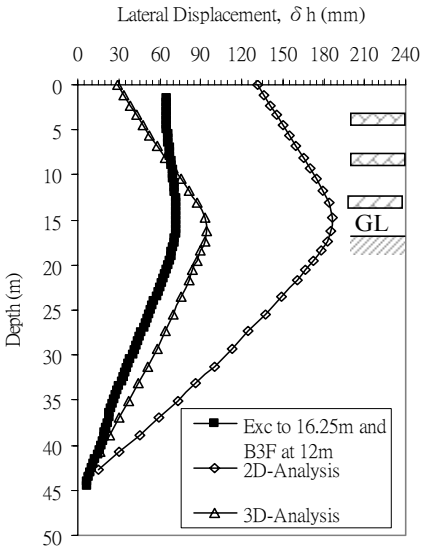

(d) 16.25m

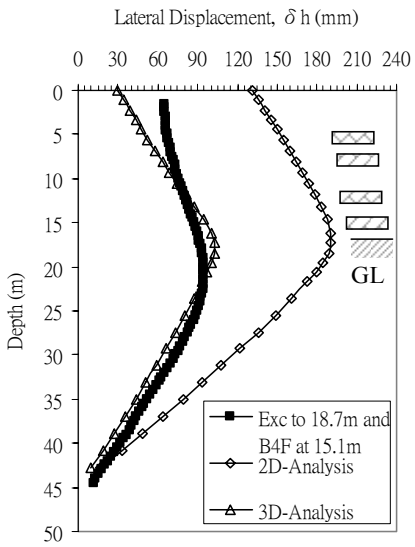

(e) 18.7m

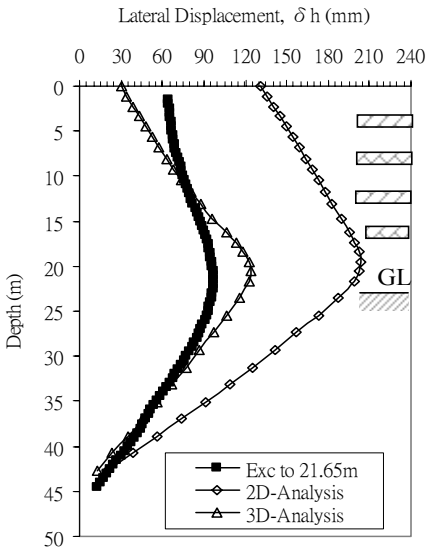

(f) 21.65m

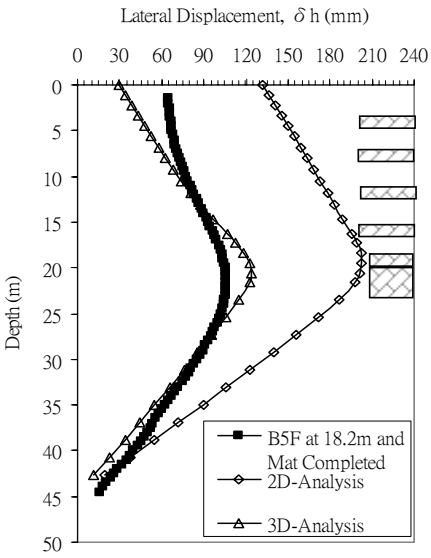

(g) 21.65m

Fig. 13 Comparisons of lateral wall movement of SI16 between measurement and numerical analyses at Podium zone for various excavation depths *H* and construction of concrete slab and mat

Table 8 Restraint effects on the lateral displacement of excavation at Podium zone (SI16)

Depth/length ratio of various excavation stage	$(\sum E_c A_c/L_c)/A$ (kN/m/m^2)	Lateral displacment of diaphragm wall			
		$(\delta_{hmax})_{observed}$ (mm)	$(\delta_{hmax})_{3D}$ (mm)	$(\delta_{hmax})_{2D}$ (mm)	PSR $(\delta_{hmax})_{3D}/(\delta_{hmax})_{2D}$
1st stage (0 ~ −5.6 m) L/H = 8.06	< 400	52.39	52.39	163.94	0.32
2nd stage (−5.6 ~ −10.05 m) L/H = 4.48	400 (B1F)	64.97	66.98	166.11	0.40
3rd stage (−10.05 ~ −13.15 m) L/H = 3.42	639 (B1F + B2F)	64.97	81.04	177.50	0.46
4th stage (−13.15 ~ −16.25 m) L/H = 2.77	776 (B1F ~ B3F)	94.89	94.28	186.49	0.51
5th stage (−16.25 ~ −18.70 m) L/H = 2.40	899 (B1F ~ B4F)	97.00	102.59	190.81	0.54
6th stage (−18.70 ~ −21.65 m) L/H = 2.08	3.99×10^6 (B1F ~ B5F and 3 m thick concrete mat)	106.27	124.11	202.99	0.61
Concrete floor slab basement supporting system at Podium zone: B1F~B5F 		(1) 3 m thick of concrete mat was constructed at the final excavation level. (2) 0.15 m thick of concrete floor slab basement (B1F~B5F) was constructed in the sequential excavation for supporting system. (3) Stiffness of supporting system: $(\sum E_c A_c/L_c)/A$ = overall axial stiffness E_c = Elastic modulus of concrete = 2.13×10^7 kPa A_c = Cross sectional area of basement floor L_c = Length of strut member L = Vertical length of diaphragm wall = 45 m			

As discussed above, the widths of primary wall L_p at excavation zone in Taipei 101 construction project are 87 m (Tower zone) and 60 m (Podium zone) and can be categorized into a wall type of intermediate width whereas the corresponding width of secondary wall L_s are 98 m (Tower zone) and 152 m (Podium zone) respectively which are much larger than 20 m. As a consequence, the aforementioned geometry configuration causes all sections being evaluated become not possible to situate at plane strain condition during the excavation and these verify the calculation from Ou, *et al* (1996). Definitely, the lateral wall movement for all sections being evaluated with $d < 1.48H$ (Tower zone) or $< 1.39H$ (Podium zone) can be restrained by the wall corner and the deformation behavior of wall system can only be captured by 3-D computation scheme.

7. CONCLUSIONS

A 3-D deformation analysis incorporated with steady state groundwater seepage calculation is capable of predicting the variation of pore water pressure and lateral wall movement during the excavation at Tower zone and Podium zone in Taipei 101 construction project. In addition, it is observed that the empirical relationship between ground settlement and lateral wall movement of deep excavation falls in the similar range to that from Ou, *et al*. (1998). However, the numerical analysis underestimates the ground settlement and the deviation can be caused by the inherent limitation of material models. The PSR values at both excavation zones reveal that the lateral wall movement of all sections being evaluated along diaphragm wall can be restrained by the wall corner during the excavation and the heavily supporting system seems hardly to suppress this effect. Eventually, it should be highlighted that the 3-D computation model is exceedingly crucial to reflect the realistic deformation behavior of deep excavation in Taipei 101 construction project.

ACKNOWLEDGEMENTS

The authors acknowledge Mr. Pei-Yuan Lin from Taipei International Financial Corporation Project, KMG-TKMG-RSEA-TYW Joint Venture, Taipei, for his kindly support on providing valuable information and instrumentation data to make this study possible.

REFERENCES

Lee, Fook-Hou, Yong, Kwet-Yew, Quan, Kevin C.N., and Chee, Kum-Thon (1998). "Effect of corners in strutted excavations: Field monitoring and case histories." *Jounal of Geotechnical and Geoenvironmental Engineering*, ASCE, 124(4), 339–348.

Lin, D. G. and Woo, S. M. (2000). "Deformation analysis of Taipei International Financial Center deep excavation project." Technical Report, Trinity Foundation Engineering Consultants Co., Ltd.

Lin, D. G., Chung, T. C., and Phienwej, N. (2003). "Quantitative evaluation of the three dimensional deformation of multi-

strutted deep excavation in soft clay ground." *Geotechnical Engineering Journal*, South East Asian Geotechnical Society, Vol. 34, No. 1, 41−57.

Lin, D. G. and Woo, S. M. (2005). "Geotechnical analyses of Taipei International Financial Center (Taipei 101) construction project." *16th International Conference on Soil Mechanics and Geotechnical Engineering*, Osaka, Japan, 1513−1516.

Liu, K. X. (1995). "Three dimensional analyses of deep excavation in soft clay." M. Eng. Thesis, National University of Singapore, Singapore.

Mana, A. I. and Clough, G. W. (1981). "Prediction of movements for braced cuts in clay." *Journal Geotechnical Engineering*, ASCE, 107, 759−777.

Itasac Consulting Group, Inc. (1999). *Manual of FLAC3D*, Version 2, 1−5.

Ou, C. Y., Hsieh, P. G., and Chiou, D. C. (1993). "Characteristics of ground surface settlement during excavation." *Can. Geotech. J.*, 30(5), 758−767.

Ou, C. Y., Liao, J. T., and Lin, H. D. (1998). "Performance of diaphragm wall constructed using top-down method." *Journal of Geotechnical and Geoenvironmental Engineering*, ASCE, 124(9), 987−808.

Ou, C. Y., Chiou, D. C., and Wu, T. S. (1996). "Three-dimensional finite element analysis of deep excavations." *Journal of Geotechnical and Geoenvironmental Engineering*, ASCE, 122(5), 337−345.

Ou, C. Y. and Shiau, B. Y. (1997). "Analysis of corner effect on excavation behaviors." *Canadian Geotech. J.*, 35, 532−540.

Peck, R. B. (1969). "Deep excavation and tunneling in soft ground." *Proceedings of the 7th International Conference on Soil Mechanics and Foundation Engineering*, Mexico, State of the Art Volume, 225−290.

Simpson, B. (1992). "Retaining structure: displacement and design." *Geotechnique*, 42(7), 541−576.

Wong, L. W. and Patron, B. C. (1993). "Settlements induced by deep excavations in Taipei." *Proc., 11th Southeast Asian Geotech. Conf.*, The Institution of Engineers, Malaysia, Kuala Lumpur, 787−791.

APPENDIX

Figures A1 and A2 present the lateral wall movement of various sections located at a distance *d* from the wall corner and the corresponding PSR value of the section in sequential excavation stage at Tower zone and Podium zone.

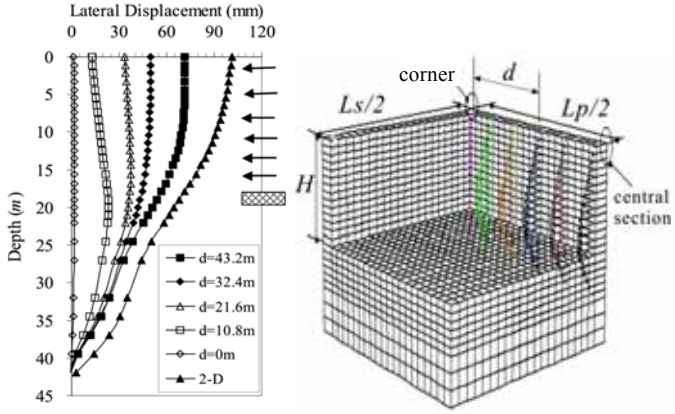

Fig. A1(a) Lateral wall movement of a section located at a distance, *d*, from corner at Tower zone for final excavation stage ($L_p \times L_s$ = 87 m × 98 m, H = 21.6 m)

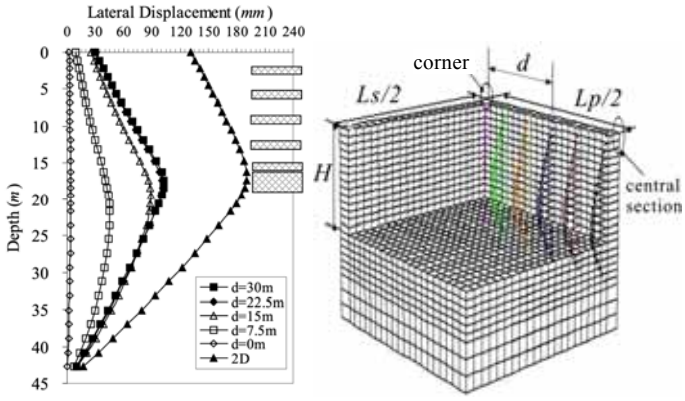

Fig. A2(a) Lateral wall movement of a section located at a distance, *d*, from corner at Podium zone for final excavation stage ($L_p \times L_s$ = 60 m × 152 m, H = 21.6 m)

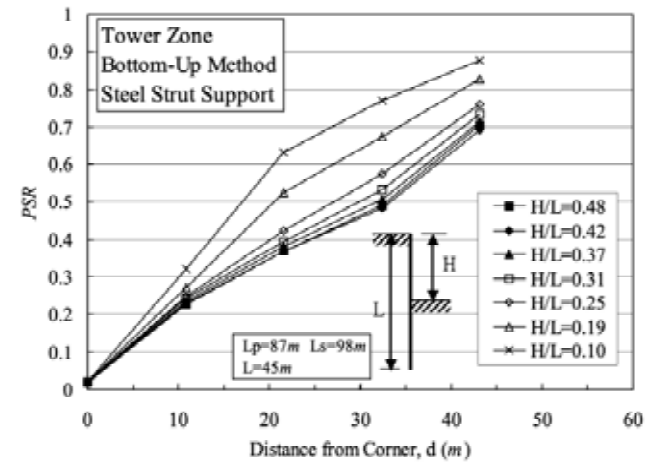

Fig. A1(b) Plane Strain Ratio (PSR) of a section located at a distance, *d*, from corner for various excavation depths *H* at Tower zone

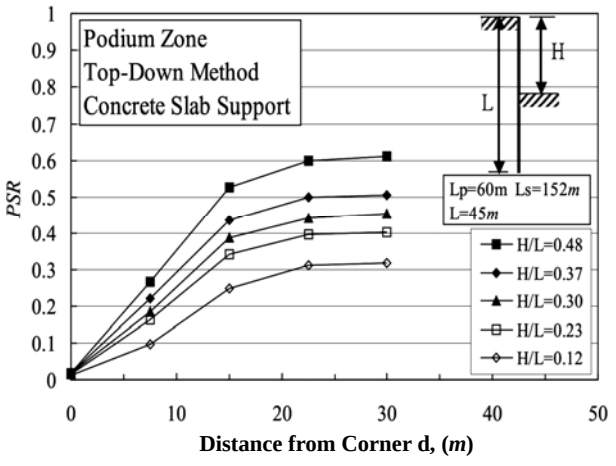

Fig. A2(b) Plane Strain Ratio (PSR) of a section located at a distance, *d*, from corner for various excavation depths at Podium zone